



# OPEN Rapid decline in extratropical Andean snow cover driven by the poleward migration of the Southern Hemisphere westerlies

Raúl R. Cordero<sup>1</sup>, Sarah Feron<sup>1,2</sup>✉, Alessandro Damiani<sup>3</sup>, Shelley MacDonell<sup>4</sup>, Jorge Carrasco<sup>5</sup>, Jaime Pizarro<sup>1</sup>, Cyrus Karas<sup>1</sup>, Jose Jorquera<sup>1</sup>, Edgardo Sepulveda<sup>1,6</sup>, Fernanda Cabello<sup>1</sup>, Francisco Fernandez<sup>7</sup>, Chenghao Wang<sup>8,9</sup>, Alia L. Khan<sup>10,11</sup> & Gino Casassa<sup>5</sup>

Seasonal snow in the extratropical Andes is a primary water source for major rivers supplying water for drinking, agriculture, and hydroelectric power in Central Chile. Here, we used estimates from the Moderate Resolution Imaging Spectroradiometer (MODIS) to analyze changes in snow cover extent over the period 2001–2022 in a total of 18 watersheds spanning approximately 1,100 km across the Chilean Andes (27–36°S). We found that the annual snow cover extent is receding in the watersheds analyzed at an average pace of approximately 19% per decade. These alarming trends have impacted meltwater runoff, resulting in historically low river streamflows during the dry season. We examined streamflow records dating back to the early 1980s for 10 major rivers within our study area. Further comparisons with large-scale climate modes suggest that the detected decreasing trends in snow cover extent are likely driven by the poleward migration of the westerly winds associated with a positive trend in the Southern Annular Mode (SAM).

**Keywords** Snow, Andes, Climate Change

Stretching over 7,200 km, the Andes hold the distinction of being the longest series of mountain ranges on Earth. The extratropical Andes, spanning from latitude 27° to latitude 36°S, boasts extensive snow-covered areas<sup>1</sup>. Regions to the north are typically affected by a drier climate, while areas to the south are restricted by the lower elevations of the range<sup>1</sup>. During the wet season, seasonal snow blankets the landscape, filling the gaps between mountaintops in the extratropical Andes. The subsequent meltwater runoff plays a crucial role in recharging groundwater and replenishing rivers and reservoirs in Central Chile during the dry season<sup>2</sup>.

Snowfall in the extratropical Andes is mainly a result of passing frontal systems, which can involve cut-off lows displaced equatorward of the primary westerly wind belt<sup>3</sup> and atmospheric rivers<sup>4</sup>. Over 90% of the snowfall in this region occurs between April and September<sup>5</sup>, when the South Pacific Anticyclonic (SPA) circulation reaches its northernmost position. The SPA is responsible for the extremely dry conditions that prevail most of the year in the northern Atacama Desert<sup>6</sup>. However, the SPA position between April and September allows moisture-laden air masses pushed by the westerlies to reach the extratropical Andes, including the southern Atacama Desert. During the austral summer, the seasonal north-south displacement of the SPA circulation pushes southward the westerly belt, leading to drier conditions in the extratropical Andes<sup>3</sup>.

Satellite-derived records indicate a rapid recession of the Andean snow<sup>7</sup>. Landsat imagery dating back to 1986 reveals a significant decline in the dry-season snow cover extent in the southern Andes (18–40°S)<sup>8–10</sup>.

<sup>1</sup>Universidad de Santiago de Chile, Av. Bernardo O'Higgins 3363, Santiago, Chile. <sup>2</sup>University of Groningen, Woldringdijk 34, Leeuwarden 8911 CE, Netherlands. <sup>3</sup>Center for Climate Change Adaptation, National Institute for Environmental Studies, Tsukuba 305-8506, Japan. <sup>4</sup>Centro de Estudios Avanzados en Zonas Áridas (CEAZA), La Serena, Chile. <sup>5</sup>University of Magallanes, Av. Manuel Bulnes 1855, Punta Arenas 621-0427, Chile. <sup>6</sup>Department of Chemical and Environmental Engineering, University of Arizona, 1133 James E. Rogers Way, Tucson, AZ 85721, USA. <sup>7</sup>Universidad Andrés Bello, Quillota 980, Viña del Mar, Chile. <sup>8</sup>School of Meteorology, University of Oklahoma, Norman, OK 73072, USA. <sup>9</sup>Department of Geography and Environmental Sustainability, University of Oklahoma, Norman, OK 73019, USA. <sup>10</sup>Western Washington University, 516 High St, Bellingham, WA 98225, USA. <sup>11</sup>National Snow and Ice Data Center, Cooperative Institute for Research in Environmental Sciences, University of Colorado—Boulder, 449 UCB University of Colorado Boulder, Boulder, CO 80309-0449, USA. ✉email: s.c.feron@rug.nl

Satellite estimates from the Moderate Resolution Imaging Spectroradiometer (MODIS), available since 2000, also indicate accelerated snow losses in the same region<sup>11,12</sup>. According to MODIS-derived estimates, the annual snow persistence decreased at a rate of up to 20% per decade over the period 2000–2016 in the extratropical Andes (23°–40°S)<sup>12</sup>. This trend is consistent with radiosonde-derived changes in the equilibrium line altitude (ELA), which has been climbing on the western side of the extratropical Andes hundreds of meters per year between 2000 and 2018<sup>13</sup>. The rapid decline in the extratropical snowpack poses a major challenge for the water security of Central Chile.

The interannual variability of the snowpack in the extratropical Andes is influenced by the El Niño–Southern Oscillation (ENSO)<sup>9,12,14</sup>. The phases of ENSO, namely El Niño and La Niña, are driven by the strength of trade winds blowing west along the equator and pushing warm water from South America toward Asia<sup>15</sup>. During El Niño events, trade winds weaken, and warm water accumulates near the west coast of the Americas. During La Niña events, trade winds strengthen, pushing more warm water toward Asia, increasing upwelling and bringing cold, nutrient-rich water to the surface<sup>16</sup>. Through atmospheric teleconnections, El Niño and La Niña influence the climate in the extratropical Andes making it wetter and drier, respectively<sup>17</sup>.

Large-scale natural climate modes, such as the Southern Annular Mode (SAM), also play a major role in precipitation and snow cover extent in the extratropical Andes<sup>9,12,14</sup>. The SAM index describes the strength and position of the circumpolar westerly winds<sup>18</sup>. A positive (negative) SAM index is associated with the strengthening (weakening) and poleward (northward) migration of the westerly winds<sup>19</sup>. Strengthened westerlies around Antarctica result in a southward displacement of the storm tracks and weather systems that typically bring precipitation to the extratropical Andes, leading to snow cover deficits in Central Chile<sup>10</sup>. The trend toward positive values of the SAM index observed since the late 1950s<sup>20</sup> appears to have played a central role in the precipitation losses seen in recent decades in the extratropical Andes<sup>21,22</sup>. The region recently experienced a megadrought, the longest in at least 1,000 years, which lowered reservoir levels and caused tensions and social unrest over water<sup>23</sup>.

Here we analyzed the changes in snow cover extent from 2001 to 2022 in a total of 18 watersheds (also called drainage basins or catchments) within Central Chile, which we grouped into three regions based on latitude: 27–31°S, 31–34°S, and 34–36°S. Our study area encompasses eight densely populated administrative 'Regions' in Chile, where the freshwater supply ultimately depends on the Andean snowpack. Snow cover data comes from MODIS/Terra Snow Cover Daily L3 Global 500 m SIN Grid, collection 6.1<sup>24</sup>. We found that the snow cover extent declined across the entire study area at an average rate of approximately 19% per decade. The consistency of our snow cover data was tested using a streamflow dataset from 10 rivers in our study area. Further comparisons involved precipitation, the SAM index, and sea surface temperatures (SST) in two Niño regions. These comparisons suggest that this decreasing trend in snow cover extent may be driven by the poleward migration of the westerly winds associated with a positive trend in the SAM index.

## Results

### Seasonal snow in Central Chile has rapidly declined

According to MODIS-derived records, the snow cover extent has declined in each of the 18 analyzed watersheds (Fig. 1a). From 2001 to 2022, the annual snow cover extent of the Putaendo basin decreased at a record rate of 28% per decade. Significant negative trends ( $p$ -value < 0.05), generally around 20% per decade, were also observed in the watersheds southward of latitude 31°S. However, as indicated in Table 1, the pace of receding of the annual snow cover extent is not statistically significant ( $p$ -value > 0.05) in the case of watersheds located in the northernmost portion of our study area (27–31°S). The absence of statistically significant trends is consistent with the relatively small changes in snow cover extent observed from 2001 to 2012 to 2013–2022 in the two northernmost watersheds, Copiapó and Huasco: +1% and –7%, respectively (Fig. 1b). In contrast, the changes in snow cover extent over the same period were considerably larger in the case of the Aconcagua (–22%), Mapocho (–24%), and Maipo (–20%) basins (Fig. 1b). The snowpack accumulated during the winter in these basins serves as a primary water source for major cities in Central Chile, including the capital city, Santiago.

The snow cover extent is receding more rapidly during the dry season than during the wet season (Table 1). The snow cover extent in our study area exhibits a distinct seasonal cycle (Figs. S1–S2). The annual peak occurs in mid-winter, and the dry season extends from late spring (October) to early fall (March). Over 90% of the snowfall in our study area takes place between April and September<sup>5</sup>. The extent of snow cover generally exhibits fewer negative trends during quarters corresponding to the wet season than during quarters corresponding to the dry season. As shown in Table 1, the winter (JJA) trends are considerably lower than the spring (SON) trends in each of the analyzed 18 watersheds. The negative trends tend to be even steeper in the last quarter of the year (OND). From 2001 to 2022, the OND snow cover extent decreased at record rates, approaching 40% per decade in major watersheds like Aconcagua (Table 1). The faster recession of the snow cover during the dry season aligns with prior research, indicating that the persistence of snow cover in the extratropical Andes (29–36°S) has decreased at an average rate of 2–5 fewer days per year<sup>12</sup>.

Record-breaking deficits in snow cover have affected the extratropical Andes in recent years (Fig. 1c). From 2018 to 2021, the snow cover extent exhibited severe and consecutive deficits in most of the 18 watersheds within our study area (Figs. S3–S6). As shown in Fig. 1c (center panel), deficits close to 40% were observed in 2019 in the most densely populated Chilean regions (31–34°S). The 2019 deficits were considerably larger in the case of the Aconcagua (–50%) and Mapocho (–60%) basins (Figs. S3–S6). The severe deficits seen from 2018 to 2021 are behind the steep negative trends in snow cover extent. Negative significant trends ( $p$ -value < 0.05) were observed in snow cover extent in the region 31–34°S (–22% per decade; Fig. 1c, center panel) and in the region 34–36°S (–17% per decade; Fig. 1c, lower panel). Although deficits in the annual snow cover extent were also seen from 2018 to 2021 in the northernmost portion of our study area, the trends are not statistically significant ( $p$ -value > 0.1) in this region 27–31°S (Fig. 1c, upper panel).

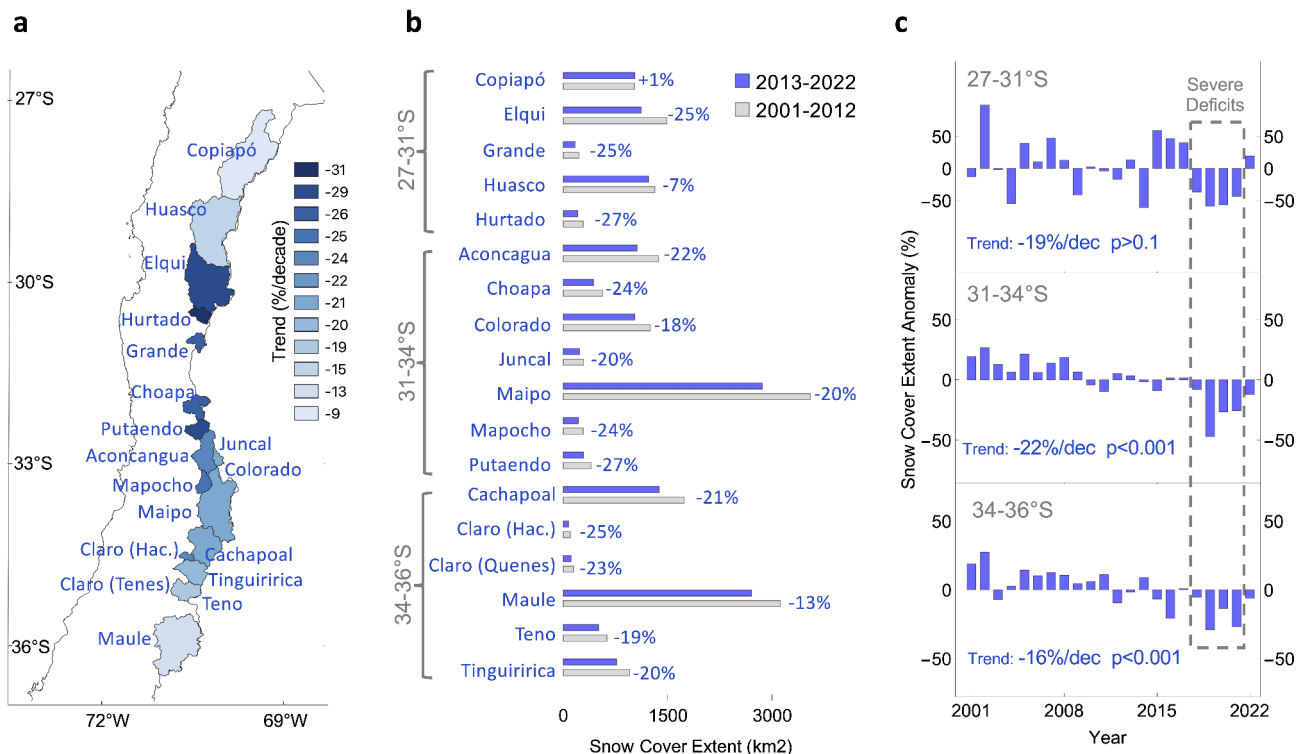


**Fig. 1.** The snow cover extent is rapidly declining in the extratropical Andes. **(a)** Trend in the annual snow cover extent of 18 watersheds (also called drainage basins or catchments) in Central Chile (from latitude 27°S to 36°S), computed from MODIS-derived estimates over the period 2001–2022. Additional statistics are shown in Table 1. **(b)** Changes in snow cover extent from 2001–2012 to 2013–2022 in 18 watersheds in Central Chile. **(c)** Annual snow cover extent relative to the 2001–2020 mean. The watersheds in **(a)** were grouped into three regions based on latitude: 27–31°S, 31–34°S, and 34–36°S. Data are based on satellite-derived estimates from MODIS/Terra Snow Cover Daily L3 Global 500 m SIN Grid, version 6.1, available at <https://nsidc.org/data/mod10a1/versions/61>. Plots were generated using Python's Matplotlib library<sup>49</sup>, version 3.4.3, <https://matplotlib.org/3.4.3/contents.html>

### Rivers in Central Chile are drying

The rapid decline in the extratropical snow cover poses a major challenge for Central Chile, as the late-spring-summer meltwater runoff from seasonal snow is the primary water source for rivers in the region. Streamflows in our study area plummeted over the past decade (Fig. S7). Data from 10 streamflow monitoring stations (Table S1) with long-term continuous records over the period 1980–2022 show that streamflows have significantly decreased in Central Chile in recent decades to historically low levels (Fig. S8). In the Aconcagua River, for example, eight of the ten lowest streamflows ever recorded occurred since 2010 (Fig. S8e). Likely responding to the negative trends in snow cover extent, dry season streamflows are also rapidly weakening (Fig. S9). From 1980 to 2022, the annual streamflow of the Maipo river decreased at a record rate of 18.7 m<sup>3</sup>/s per decade. Negative significant trends ( $p$ -value < 0.05) were found in the annual streamflows of each of the 10 rivers analyzed (Table S2).

The snow cover extent in spring drives the subsequent dry season river streamflow. We found a strong correlation ( $R > 0.8$ ,  $p < 0.001$ ) between the dry season (NDJF) river streamflow and the spring (SON) snow cover extent of the corresponding basin (Fig. S10). Similar strong correlations were found when comparing the dry season (NDJF) river streamflow and the monthly averages of the spring snow cover extent (Table S3). For example, the correlation between the dry season streamflow of the Maipo river and the September snow cover extent in the Maipo watershed is about 0.7 ( $p$ -value  $\sim 0.001$ ) (Table. S3). The strong coupling between the snow cover extent in spring months and the dry season streamflow supports the consistency of our snow cover estimates and provides predictability for the river streamflow several months in advance.

### Droughts in Central Chile have become recurrent

The last decade was the driest ever recorded in Central Chile with average deficits in precipitation close to 30% in the most densely populated Chilean regions (31–34°S) (Fig. 2a). These deficits not only contributed to the snow cover losses, but also exacerbated water stress, causing tensions and social unrest over water in the northernmost regions of our study area, where water scarcity is endemic<sup>25</sup>. Precipitation in our study area exhibits a sharp meridional gradient, increasing as one moves southward from a few tens of millimeters per year in the southern part of the Atacama Desert (27–31°S) to several meters per year in the fertile valleys of Central Chile (34–36°S) (Fig. 2b).

	Basin ↓	Annual		AMJ		MJJ		JJA		JAS		ASO		SON		OND	
		Trend (%/dec)	p-value	Trend (%/dec)	p-value	Trend (%/dec)	p-value	Trend (%/dec)	p-value	Trend (%/dec)	p-value	Trend (%/dec)	p-value	Trend (%/dec)	p-value	Trend (%/dec)	p-value
27-31°S	Copiapo	-9	0.654	-16	0.461	-11	0.589	3	0.879	-4	0.868	-6	0.800	-28	0.356	-28	0.370
	Elqui	-28	<b>0.046</b>	-28	0.103	-18	0.190	-16	0.218	-26	0.097	-37	<b>0.031</b>	-45	<b>0.031</b>	-45	0.093
	Grande	-26	<b>0.008</b>	-30	0.131	-15	0.198	-10	0.267	-18	<b>0.031</b>	-31	<b>0.008</b>	-42	<b>0.010</b>	-57	<b>0.027</b>
	Huasco	-15	0.366	-18	0.284	-10	0.496	-3	0.831	-13	0.489	-19	0.356	-27	0.285	-26	0.429
	Hurtado	-30	<b>0.026</b>	-42	<b>0.031</b>	-22	0.163	-18	0.158	-22	0.089	-35	<b>0.019</b>	-41	<b>0.027</b>	-47	0.070
31-34°S	Aconcagua	-23	<b>0.000</b>	-38	<b>0.016</b>	-20	<b>0.028</b>	-11	<b>0.035</b>	-7	<b>0.013</b>	-11	<b>0.005</b>	-21	<b>0.000</b>	-37	<b>0.000</b>
	Choapa	-26	<b>0.000</b>	-39	<b>0.021</b>	-21	0.028	-12	0.049	-10	0.014	-16	0.010	-31	0.001	-53	0.001
	Colorado	-19	<b>0.000</b>	-33	<b>0.015</b>	-18	<b>0.030</b>	-10	<b>0.043</b>	-6	<b>0.006</b>	-8	<b>0.003</b>	-16	<b>0.000</b>	-27	<b>0.000</b>
	Juncal	-21	<b>0.000</b>	-35	<b>0.023</b>	-16	0.076	-7	0.207	-3	0.102	-5	<b>0.024</b>	-16	<b>0.000</b>	-31	<b>0.000</b>
	Maipo	-20	<b>0.000</b>	-32	<b>0.017</b>	-16	0.058	-8	0.109	-6	<b>0.005</b>	-8	<b>0.001</b>	-17	<b>0.000</b>	-30	<b>0.000</b>
	Mapocho	-25	<b>0.000</b>	-38	<b>0.049</b>	-20	0.054	-13	0.068	-12	<b>0.019</b>	-18	<b>0.002</b>	-31	<b>0.000</b>	-48	<b>0.000</b>
	Putendo	-28	<b>0.000</b>	-39	<b>0.026</b>	-24	<b>0.013</b>	-16	<b>0.020</b>	-15	<b>0.010</b>	-21	<b>0.006</b>	-35	<b>0.001</b>	-55	<b>0.001</b>
34-36°S	Cachapoal	-20	<b>0.000</b>	-33	<b>0.014</b>	-16	0.051	-8	0.155	-6	<b>0.009</b>	-7	<b>0.003</b>	-13	<b>0.000</b>	-23	<b>0.000</b>
	Claro (Hacienda)	-24	<b>0.000</b>	-37	0.054	-19	0.094	-13	0.109	-10	<b>0.034</b>	-10	<b>0.019</b>	-14	<b>0.003</b>	-24	<b>0.001</b>
	Claro (Los Quenes)	-22	<b>0.000</b>	-37	<b>0.019</b>	-26	<b>0.017</b>	-19	<b>0.031</b>	-12	0.051	-8	0.111	-13	<b>0.017</b>	-21	<b>0.011</b>
	Maule	-12	<b>0.001</b>	-14	0.189	-7	0.309	-6	0.247	-4	0.260	-4	0.158	-11	<b>0.033</b>	-24	<b>0.010</b>
	Teno	-19	<b>0.000</b>	-27	<b>0.048</b>	-15	0.059	-10	0.088	-8	<b>0.035</b>	-8	<b>0.026</b>	-14	<b>0.004</b>	-25	<b>0.004</b>
	Tinguiririca	-19	<b>0.000</b>	-30	<b>0.013</b>	-16	<b>0.030</b>	-9	0.099	-6	<b>0.023</b>	-6	<b>0.014</b>	-11	<b>0.003</b>	-20	<b>0.002</b>

**Table 1.** Trends over the period 2001–2022 in the snow cover extent. Trends considered significant (p-value < 0.05) are highlighted in bold. Trends are based on satellite-derived estimates from MODIS/Terra Snow Cover Daily L3 global 500 m SIN Grid, version 6.1. For more information see figs. S2–S3.

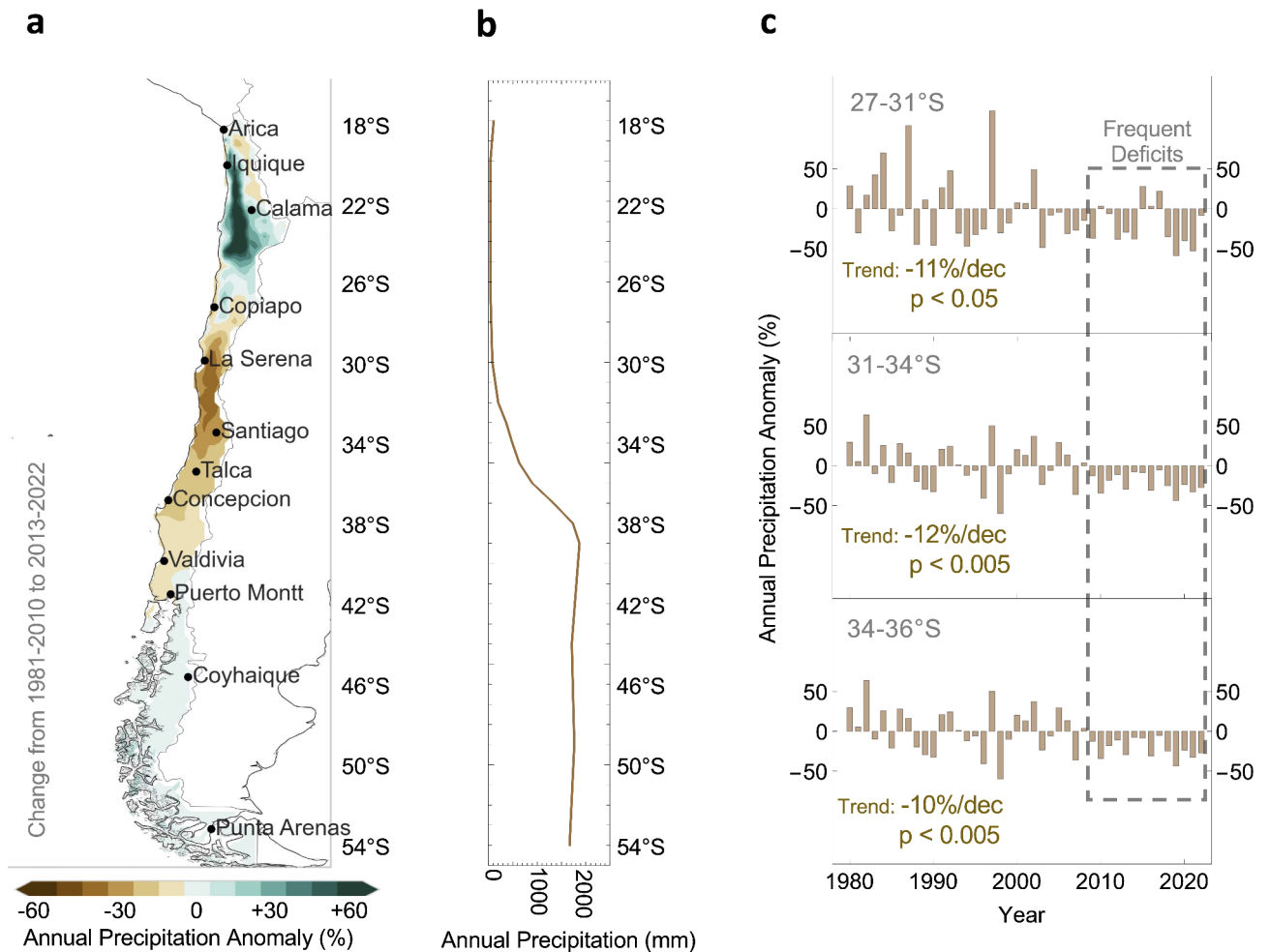


**Fig. 2.** The extratropical Andes have experienced frequent precipitation deficits over the past decade. (a) Changes, from 1981–2010 to 2013–2022, in annual precipitation. (b) Annual precipitation (1981–2010) in Chile shows a pronounced meridional gradient, increasing as moving southwards. (c) Annual precipitation relative to the 1981–2010 mean in three regions: 27–31°S, 31–34°S, and 34–36°S. The dotted rectangular box highlights the period of frequent deficits that began in 2008. Data come from the ERA5 reanalysis<sup>48</sup> available at <https://www.ecmwf.int/en/forecasts/datasets/reanalysis-datasets/era5>. Plots were generated using Python's Matplotlib library<sup>49</sup>, version 3.4.3, <https://matplotlib.org/3.4.3/contents.html>.

The extratropical Andes have experienced frequent and prolonged dry spells, especially since 2008 (Fig. 2c). From 2008 to 2022, precipitation exhibited severe and consecutive deficits southward of latitude 31°S. As shown in Fig. 2c (center panel), deficits larger than 50% were observed in 2019 in the most densely populated Chilean regions (31–34°S). 2019 was the driest year seen in these regions in at least 50 years. Negative significant trends ( $p$ -value  $< 0.05$ ) have been observed over the period 1980–2022 in the region 27–31°S (-11% per decade; Fig. 2c, upper panel), in the region 31–34°S (-12% per decade; Fig. 2c, center panel), and in the region 34–36°S (-10% per decade; Fig. 2c, lower panel). The recurring deficits in annual precipitation have resulted in a severe megadrought in Central Chile<sup>23</sup>.

### The ENSO footprint in the decline of snow in Central Chile is not apparent

Frequent La Niña events in the last 25 years have likely affected both precipitation and snow cover in the extratropical Andes. Through atmospheric teleconnections, El Niño and La Niña influence the climate in the extratropical Andes, making it wetter and drier, respectively<sup>17</sup>. Two of the Niño regions currently monitored by NOAA's CPC are the Niño 1 + 2 Region (right in front of the western coast of Peru; 0–10°S, 90°W–80°W) and the Niño 3.4 Region (in the tropical central Pacific; 5°N–5°S, 170°W–120°W) (Fig. 3a). El Niño/La Niña events are classified according to SST anomalies exceeding the  $\pm 0.5$  °C threshold in the Niño 3.4 Region<sup>15</sup>. Since 1998 we have seen two triple-dip La Niña's that spanned the years 1998–2001 and 2020–2023. Other La Niña events were recorded in 2005–2006, 2007–2009, 2010–2012, and 2016–2018 (Fig. 3b). With few exceptions, Central Chile experienced severe droughts during those years.

Despite the frequent occurrence of La Niña events in the last 25 years, SST in the Niño regions monitored by NOAA's CPC shows no significant trend. This is because, although El Niño events are less frequent, they tend to



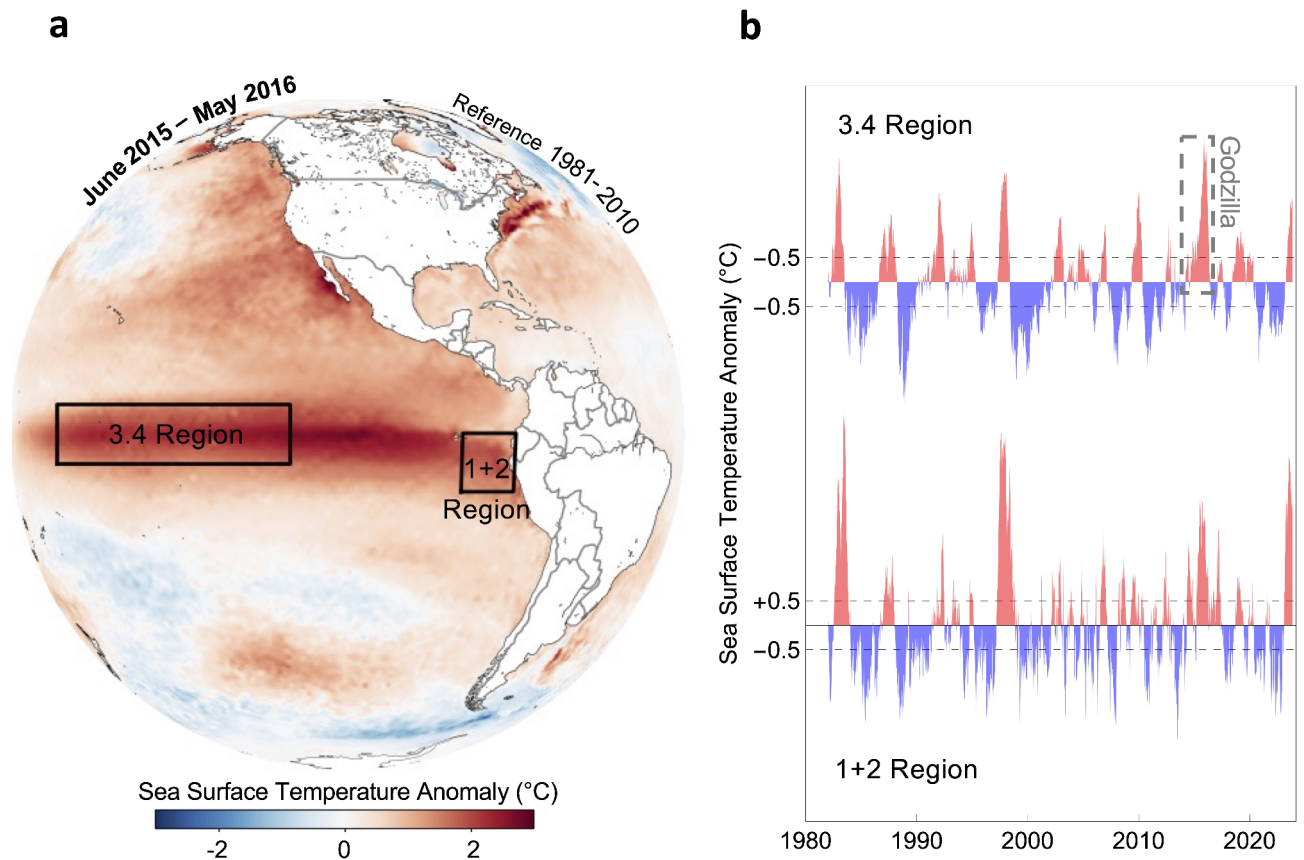


**Fig. 3.** The signature of ENSO on the decline of the Andean snow is not apparent. **(a)** Sea surface temperature (SST) anomalies during the El Niño Godzilla event (June 2015 – May 2016). The two main Niño regions currently monitored by NOAA's CPC, the Niño 1 + 2 Region (right in front of the western coast of Peru; 0–10°S, 90°W–80°W) and the Niño 3.4 Region (in the tropical central Pacific; 5°N–5°S, 170°W–120°W), are shown in the plot. **(b)** Weekly anomalies of the sea surface temperature (SST) in two important Niño regions. The dotted rectangular box in the upper panel highlights the 2015 El Niño event, often referred to as El Niño Godzilla. The SST shows no significant trend in these two important Niño regions. SST anomalies in **(a)** come from the ERA5 dataset produced by the European Centre for Medium-range Weather Forecasts (ECMWF)<sup>48</sup> available at <https://www.ecmwf.int/en/forecasts/datasets/reanalysis-datasets/era5>. Weekly SST anomalies in **(b)** come from the Climate Prediction Center (CPC), part of the National Oceanic and Atmospheric Administration (NOAA) available at <https://www.cpc.ncep.noaa.gov/data/indices/wksst8110.for>. Plots were generated using Python's Matplotlib library<sup>49</sup>, version 3.4.3, <https://matplotlib.org/3.4.3/contents.html>.

be more intense than La Niña events. For instance, the dotted rectangular box in Fig. 3b (upper panel) highlights the 2015 El Niño event, often referred to as El Niño Godzilla due to its record intensity in the Niño 3.4 region. The lack of significant trends in SST of the Niño regions makes it unlikely for ENSO to be the primary driver behind the rapid decline in seasonal snow observed in Central Chile in recent decades.

### The SAM index has become persistently positive

The persistent trend towards positive values of the SAM index is likely affecting both precipitation and snow cover in the extratropical Andes. Significant positive trends (p-value < 0.05) have been observed between 1980 and 2022 in both the annual SAM index (+0.12 per decade; Fig. 4a, upper panel) and the SAM index averaged for March–April–May–June (MAMJ) (+0.15 per decade; Fig. 4a, lower panel). The SAM's positive phase is associated with the strengthening and poleward migration of the westerly winds<sup>19</sup>, resulting in a southward displacement of the storm tracks that typically bring precipitation to the extratropical Andes. Previous studies<sup>21,22</sup> have shown that precipitation losses in Central Chile in recent decades are partially attributed to a trend towards positive values of the SAM index.

In the last decade, significant positive anomalies in the near-surface wind speed were observed during fall (March–April–May, MAM) and early winter (June, J) around Antarctica, particularly along the South Pacific sector (Fig. 4b). The intensified MAMJ westerly winds around Antarctica over the period 2013–2022 are consistent with the frequently positive values of the SAM index shown in Fig. 4a (lower panel) over the same period. The trend towards strengthened and poleward shifted westerlies (i.e., positive SAM index values) has been partially attributed to Antarctic ozone depletion<sup>26</sup>, which primarily influences the SAM index and westerly winds during the summer months<sup>21,22</sup>. This is why the success of the Montreal Protocol and the onset of ozone

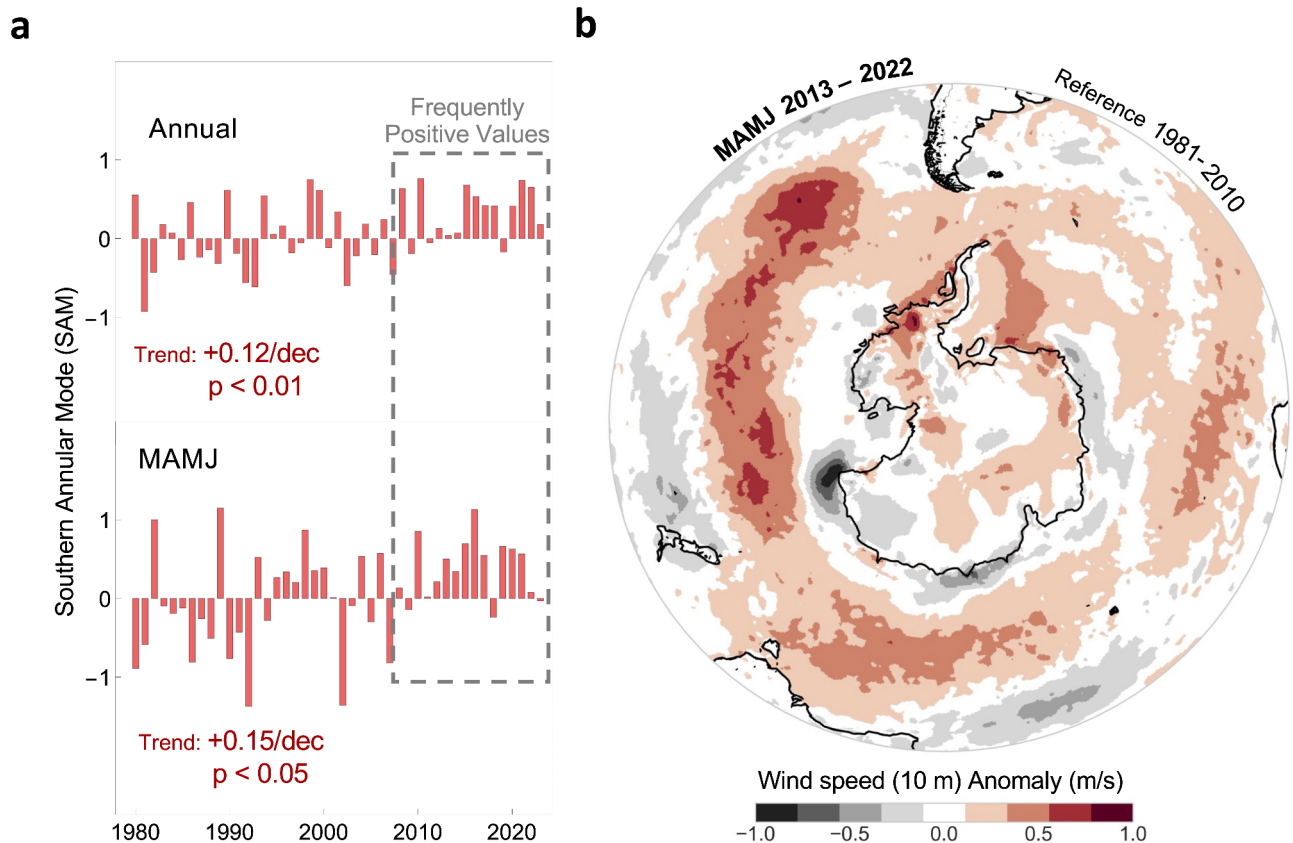


**Fig. 4.** The Southern Annular Mode (SAM) index appears to be becoming increasingly positive. **(a)** Time series of the Southern Annular Mode (SAM) index. Annual mean (upper plot) and mean SAM index for March–April–May–June (MAMJ) (lower plot). The dotted rectangular box highlights the period of frequent positive SAM values that began in 2008. **(b)** Near-surface wind speed averaged from March to June 2013–2022, relative to the 1981–2010 mean. The weakened MAMJ winds across our study area is apparent in the plot. In addition, the strengthened MAMJ westerly winds around Antarctica seen over the period 2013–2022 are consistent with the consistently positive values of the SAM index shown in **(a)**. Estimates of the SAM index were obtained from Climate Prediction Center (National Weather Service, National Oceanic and Atmospheric Administration – NOAA), available at: [https://www.cpc.ncep.noaa.gov/products/precip/CWlink/daily\\_ao\\_index/ao/ao.shtml#publication](https://www.cpc.ncep.noaa.gov/products/precip/CWlink/daily_ao_index/ao/ao.shtml#publication). Near-surface wind speed data in **(b)** come from the ERA5 dataset produced by the European Centre for Medium-range Weather Forecasts (ECMWF)<sup>48</sup> available at <https://www.ecmwf.int/en/forecasts/datasets/reanalysis-datasets/era5>. Plots were generated using Python's Matplotlib library<sup>49</sup>, version 3.4.3, <https://matplotlib.org/3.4.3/contents.html>.

recovery resulted in a pause in the summertime strengthening of westerlies<sup>27</sup>. Yet, the trend towards positive values of the SAM index has persisted, primarily driven by frequently positive values from March to June (Fig. 4a, lower panel).

### The decline in snow cover extent is linked to a poleward shift of the westerlies

The significant reductions in snow cover extent observed in the extratropical Andes in recent years coincided with persistently positive values of the SAM index and remarkable dry spells. As expected, we found a high correlation ( $R > +0.7$ ;  $p < 0.01$ ) between snow cover extent and precipitation (Fig. 5), which suggests that the primary driver of the decline in snow cover extent in Central Chile is the lack of snowfalls. We also found that recent losses in both precipitation and snow cover are associated with the strengthening and poleward migration of the westerlies (i.e., the trend towards positive values of the SAM index) and the southward displacement of synoptic-scale eddies traveling within the westerly flow. As shown in Fig. 5; Table 2, in each of the analyzed regions (27–31°S, 31–34°S, and 34–36°S), we found a significant anticorrelation ( $R < -0.5$ ;  $p < 0.05$ ) between snow cover extent and the SAM index. These results add evidence that, in the extratropical Andes, long-term negative trends in precipitation appear to be dominated by the poleward shift of the westerlies and the resulting trend towards positive values of the SAM index (Fig. 4).

ENSO and SST in the tropical central Pacific play a relevant role in the interannual variability of snow cover extent in the extratropical Andes, particularly southward of latitude 31°S. We found that, in two of the analyzed regions (31–34°S and 34–36°S), there is a significant correlation between the snow cover extent and SST anomalies in the Niño 3.4 region ( $R \sim +0.4$ ;  $p < 0.05$ ; Fig. 5). However, this is not the case in the northernmost

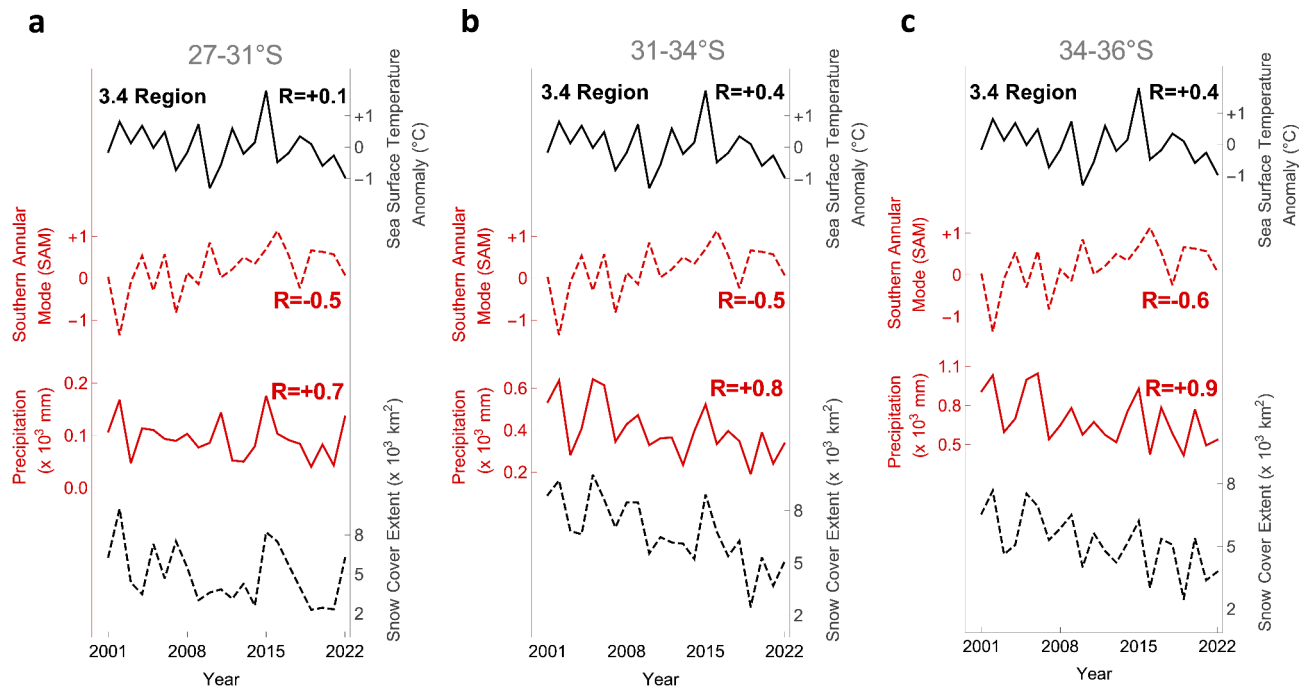


**Fig. 5.** The snow cover extent in the extratropical Andes is connected with the SAM index. Times series of snow cover extent (black dotted line) and precipitations (red line), in the following regions: **(a)** 27–31°S, **(b)** 31–34°S, and **(c)** 34–36°S. The times series of the Southern Annular Mode (SAM) index (red dotted line), and sea surface temperature (SST) anomalies in the Niño 3.4 region (black line) are also shown for comparisons. The correlation coefficients between the snow cover extent and the precipitations, the SAM index, and the SST anomalies in the Niño 3.4 region are indicated in the plots. Additional basin-level statistics are presented in Table 2. As shown in Table 2, the correlations between the snow cover extent and the SST in the Niño 1 + 2 region are not significant. Snow cover data (averaged from September to December) are based on satellite-derived estimates from MODIS/Terra Snow Cover Daily L3 Global 500 m SIN Grid, version 6.1, available at <https://nsidc.org/data/mod10a1/versions/61>. Precipitation data (averaged from June to September) come from the ERA5 reanalysis<sup>48</sup> available at <https://www.ecmwf.int/en/forecasts/datasets/reanalysis-datasets/era5>. Weekly SST anomalies in the Niño 3.4 region (averaged from August to September) come from the Climate Prediction Center (CPC), part of the National Oceanic and Atmospheric Administration (NOAA) available at <https://www.cpc.ncep.noaa.gov/data/indices/wksst8110.for>. Estimates of the SAM index (averaged from March to June) were obtained from Climate Prediction Center (National Weather Service, National Oceanic and Atmospheric Administration – NOAA). Daily estimates of the SAM index are available at: [https://www.cpc.ncep.noaa.gov/products/precip/CWlink/daily\\_ao\\_index/aao/aao.shtml#publication](https://www.cpc.ncep.noaa.gov/products/precip/CWlink/daily_ao_index/aao/aao.shtml#publication). Plots were generated using Python's Matplotlib library<sup>49</sup>, version 3.4.3, <https://matplotlib.org/3.4.3/contents.html>.

region of our study area (27–31°S), where the correlation between snow cover extent and SST anomalies in the Niño 3.4 region was found to be insignificant. Nevertheless, it is unlikely that ENSO plays no role in this region. Although they are not always concurrent, La Niña (El Niño) events more frequently coincide with positive (negative) phases of SAM than expected by chance<sup>28</sup>. The relationship between SAM and ENSO suggests that the frequently positive values of the SAM index recorded in recent decades may be influenced by the frequent occurrence of La Niña events over the same period.

## Discussion

We found that the snow cover extent is receding in each of the watersheds analyzed at an average pace of approximately 19% per decade. Although these trends are based on relatively short time series (MODIS-derived data are available since late 2000 only), we have shown that they are consistent with similarly alarming trends observed since the early 1980s in both precipitations and the streamflow of major rivers in our study area. We also found that prolonged dry spells have led to severe snow cover deficits (nearly 40%) in recent years, affecting major watersheds and increasing water stress in the most densely populated region of Chile (31–34°S).

The rapid decline in extratropical Andean snow poses a significant challenge for Central Chile, as seasonal snow serves as a primary water source for major rivers, supplying water for drinking, agriculture, mining, and hydroelectric power in the region<sup>2</sup>. As the water demand steadily increases, the recurrent deficits in snow cover extent exacerbate water stress, causing tensions and social unrest over water<sup>25</sup>. As with other climate-related impacts, increasing water stress disproportionately affects vulnerable rural populations and minorities. Drying rivers in the extratropical Andes are seriously threatening rural, often indigenous, communities leading to migration and depopulation, especially in the northernmost part of our study area<sup>29</sup>.



Snow cover extent ↓	Precipitation		SAM index		SST ENSO 3.4		SST ENSO 1 + 2	
	R	p-value	R	p-value	R	p-value	R	p-value
Region I (27–31°S)	<b>+0.7</b>	<b>0.00</b>	<b>-0.5</b>	<b>0.03</b>	+0.1	0.76	+0.1	0.58
Copiapo Basin	<b>+0.6</b>	<b>0.01</b>	<b>-0.5</b>	<b>0.02</b>	+0.1	0.84	+0.2	0.43
Elqui Basin	<b>+0.7</b>	<b>0.00</b>	<b>-0.5</b>	<b>0.02</b>	+0.2	0.32	+0.2	0.35
Grande Basin	<b>+0.8</b>	<b>0.00</b>	<b>-0.6</b>	<b>0.02</b>	+0.2	0.28	+0.2	0.37
Huasco Basin	<b>+0.7</b>	<b>0.00</b>	-0.3	0.20	+0.2	0.36	+0.2	0.41
Hurtado Basin	<b>+0.7</b>	<b>0.00</b>	<b>-0.5</b>	<b>0.02</b>	+0.2	0.47	+0.2	0.49
Region II (31–34°S)	<b>+0.8</b>	<b>0.00</b>	<b>-0.5</b>	<b>0.03</b>	<b>+0.4</b>	<b>0.05</b>	+0.4	0.10
Aconcagua Basin	<b>+0.8</b>	<b>0.00</b>	<b>-0.5</b>	<b>0.03</b>	+0.4	0.10	+0.3	0.12
Choapa Basin	<b>+0.8</b>	<b>0.00</b>	<b>-0.5</b>	<b>0.02</b>	+0.3	0.17	+0.3	0.17
Colorado Basin	<b>+0.8</b>	<b>0.00</b>	<b>-0.5</b>	<b>0.02</b>	<b>+0.5</b>	<b>0.03</b>	+0.4	0.08
Juncal Basin	<b>+0.8</b>	<b>0.00</b>	<b>-0.5</b>	<b>0.04</b>	+0.4	0.08	+0.4	0.11
Maipo Basin	<b>+0.8</b>	<b>0.00</b>	<b>-0.4</b>	<b>0.03</b>	<b>+0.5</b>	<b>0.02</b>	+0.4	0.08
Mapocho Basin	<b>+0.9</b>	<b>0.00</b>	<b>-0.5</b>	<b>0.03</b>	+0.4	0.06	+0.3	0.19
Putaendo Basin	<b>+0.8</b>	<b>0.00</b>	<b>-0.5</b>	<b>0.02</b>	+0.3	0.15	+0.3	0.15
Region III (34–36°S)	<b>+0.9</b>	<b>0.00</b>	<b>-0.6</b>	<b>0.01</b>	<b>+0.4</b>	<b>0.04</b>	+0.3	0.21
Cachapoal Basin	<b>+0.8</b>	<b>0.00</b>	<b>-0.5</b>	<b>0.03</b>	<b>+0.5</b>	<b>0.02</b>	+0.4	0.09
Claro (Hacienda) Basin	<b>+0.8</b>	<b>0.00</b>	<b>-0.5</b>	<b>0.03</b>	+0.3	0.12	+0.3	0.19
Claro (Los Quenes) Basin	<b>+0.8</b>	<b>0.00</b>	<b>-0.6</b>	<b>0.00</b>	+0.3	0.12	+0.2	0.32
Maule Basin	<b>+0.9</b>	<b>0.00</b>	<b>-0.6</b>	<b>0.00</b>	+0.4	0.10	+0.2	0.45
Teno Basin	<b>+0.9</b>	<b>0.00</b>	<b>-0.5</b>	<b>0.01</b>	<b>+0.5</b>	<b>0.03</b>	+0.3	0.12
Tinguiririca Basin	<b>+0.8</b>	<b>0.00</b>	<b>-0.5</b>	<b>0.04</b>	<b>+0.5</b>	<b>0.02</b>	<b>+0.4</b>	<b>0.05</b>

**Table 2.** Correlation coefficients (R) and p-values between the snow cover extent and other variables (precipitation and climate indexes). Correlations considered significant (p-value < 0.05) are highlighted in bold.

In the Andean region, snow cover losses act as a positive feedback loop amplifying the predominant drying trends. As the snow cover declines, the surface reflects less shortwave radiation to space due to drops in the albedo, which leads to additional warming<sup>30</sup>. Less snow means there are more dark-colored surfaces to absorb energy and warm up the local environment. This positive feedback causes more snow to melt and opens even more dark surfaces for warming. In addition, prolonged multi-week dry spells frequently seen since 2008 in our study area enable aerosols deposition, which makes the snow surface dirty, further reducing its albedo. Black carbon deposition, for example, has been found to considerably darken the snow in the extratropical Andes, reducing the albedo, and accelerating melting<sup>31,32,33</sup>.

Our comparisons with large-scale climate modes (i.e., ENSO and SAM) suggest that the detected decreasing trends in snow cover extent are likely driven by the poleward migration of the westerly winds associated with a positive trend in the SAM index. We found a significant anticorrelation between the SAM index and the snow cover extent in extratropical Andes. The persistently positive phase of the SAM seen in recent years is associated with the southward displacement of the storm tracks that typically bring precipitation to the region, leading to dry spells and historic deficits in snow cover in our study area. Yet, the positive trend in the SAM index may not be the only factor contributing to the decreasing trends in snow cover extent observed in recent decades. For example, experiments conducted with two atmospheric models have suggested that upper ocean warming over the subtropical southwest Pacific (SSWP), known as the Southern Blob, may also be contributing to the drying of our area of interest<sup>34</sup>.

Although we found that phases of ENSO (i.e., El Niño and La Niña) influence the interannual variability of the extratropical Andean (especially southward of latitude 31°S), the lack of significant trends in SST of the Niño regions makes it unlikely for ENSO to be the primary driver behind the rapid decline in seasonal snow observed in Central Chile in recent decades. Yet, changes in the phase of ENSO often lead to large-scale planetary waves that affect the strength of the polar vortex<sup>35</sup> and in turn the SAM index and the circumpolar westerly winds<sup>36</sup>.

The strength of the polar vortex (i.e., stratospheric circulation) may be influencing the tropospheric westerly winds and in turn the snow cover changes in the extratropical Andes. Indeed, stratospheric variability plays an important role in driving the near-surface climate<sup>37</sup>. Accordingly, and as shown in Fig. S11, we found a strong correlation between the strength of the tropospheric westerlies (averaged for MAMJ) and the corresponding wind speeds in the polar-front jet stream (the polar vortex is the region poleward of the jet). These results denote a robust stratosphere-troposphere coupling and suggest that, by influencing the circumpolar tropospheric westerly winds, a strengthened polar vortex may have played a role in the recent snow cover losses in the extratropical Andes. So, the question arises: what has caused the polar vortex to strengthen? Although the main driver behind the MAMJ strengthening of the polar vortex seen in recent years may be in the tropics (i.e., changes in the phase of ENSO), the processes that determine the planetary wave activity are not fully understood. Further research

is needed to explore the influence of the stratospheric circulation on the year-to-year snow cover variability in the extratropical Andes.

Our results add to the growing body of evidence suggesting that trends in snow cover extent in the extratropical Andes are influenced by SAM, with ENSO playing a role in the interannual variability. However, the response (i.e., trends and year-to-year changes) of these large-scale climate modes (ENSO and SAM) to climate change is highly uncertain. It is unknown how the ENSO may change under future greenhouse warming<sup>38</sup>. Climate models suggest that under a likely emission scenario, extreme El Niño frequency will increase linearly with the global mean temperature towards a doubling at 1.5 °C warming<sup>39</sup>. An increase in the number of ‘strong’ El Niño events may boost the interannual snow cover variability. Regarding the SAM, how the strength and position of the circumpolar westerly winds will play out as the world warms remains to be seen. Yet, westerlies are projected to intensify during the 21st century under high greenhouse gas forcing<sup>40,41</sup>. This may result in further snow cover losses for Central Chile in the future.

## Methods and datasets

We calculated monthly averages of snow cover extent over the period 2001–2022 for a total of 18 basins within Central Chile. These basins were grouped into three regions based on latitude: 27–31°S, 31–34°S, and 34–36°S. Snow cover extent data are based on satellite-derived estimates from MODIS/Terra Snow Cover Daily L3 Global 500m SIN Grid, collection 6.1<sup>42</sup>, available at <https://nsidc.org/data/mod10a1/versions/61>. The Level-3 (L3) data set provides a daily composite of snow cover and albedo derived from the ‘MODIS/Terra Snow Cover 5-Min L2 Swath 500m’ data set (DOI:[https://doi.org/10.5067/MODIS/MOD10\\_L2.061](https://doi.org/10.5067/MODIS/MOD10_L2.061)). To address the need for a cloud-reduced or cloud-free daily products, a daily cloud-gap-filled (CGF) snow-cover algorithm was developed for MODIS C6.1 processing<sup>43</sup>. The biggest limitation to the use of the MODIS snow-cover products is cloud cover. Although uncertainties are site dependent<sup>44</sup>, the overall absolute accuracy of the well-studied 500 m resolution swath (MOD10\_L2) products is about 93%<sup>42</sup>. Yet, recent efforts focused on the western US have shown higher accuracy of Terra products compared with Aqua products<sup>43</sup>.

MODIS snow-cover products provide Normalized Difference Snow Index (NDSI) values from 0 to 100. There are flag values for other features in a scene (e.g., clouds). The NDSI is defined as the difference between the observed reflectance in the visible part of the spectrum (MODIS band 4, 0.555 µm) and a band in the shortwave infrared part of the spectrum (MODIS band 6, 1,640 µm), divided by the sum of both<sup>45</sup>. The snow-covered surface has a higher reflectance in the visible bands than in the shortwave infrared bands. Higher NDSI values suggest the presence of snow. In order to build up binary snow cover maps, here we used a NDSI threshold of 0.12 together with a flag system. Only estimates with a NDSI Snow Cover Basic Quality Assurance (QA) of “ok”, “good”, or “best” were used. Although the NDSI threshold can vary depending on the region and other factors, a threshold of 0.12 resulted in the highest correlation between spring snow cover extent and dry season river streamflows (Table S3). Streamflow data from 10 monitoring stations operated by the Dirección General de Aguas (DGA) were used to test the consistency of our snow cover estimates (i.e., the threshold of 0.12).

As previously shown by studies that used isotope and ionic analyses as natural water tracers<sup>46</sup>, river streamflows during the dry season in our area of interest are primarily attributable to meltwater runoff from the snowpack accumulated during the wet season. This is why a relatively high correlation between spring snow cover extent and dry season river streamflows was expected, and why streamflow data can be used to test the consistency of snow cover estimates. If the latter were considerably biased, the correlations shown in Table S3 between spring snow cover extent and dry season river streamflows would be significantly weaker. We used data from 10 monitoring stations operated with long-term continuous records over the period 1980–2022 (Table S1), available at <http://explorador.cr2.cl/>. Stations with data gaps accounting for more than 35% of the time series were not considered.

For computing the slope-adjusted snow cover extent, we used the Shuttle Radar Topography Mission (SRTM) Digital Elevation Model (DEM)<sup>47</sup>. We reprojected the DEM to the UTM zone 19 S (EPSG:5361), corresponding to the study area, using the Geographic Information System (GIS) provided by QGIS version 3.18 (<https://qgis.org/>). We then converted the DEM with the “Real Surface Area” tool from the System for Automated Geoscientific Analyses (SAGA) module, which rendered the actual surface for each snow-covered pixel.

Additional comparisons involved the precipitation in our study area, the SAM index, and SST in the Niño regions. Precipitation data come from the atmospheric reanalysis ERA5 produced by the European Centre for Medium-range Weather Forecasts (ECMWF)<sup>48</sup>, available at: <https://www.ecmwf.int/en/forecasts/datasets/reanalysis-datasets/era5>. Weekly SST anomalies in the Niño regions come from NOAA’s Climate Prediction Center (CPC), available at <https://www.cpc.ncep.noaa.gov/data/indices/wksst8110.for>. Daily estimates of the SAM index also comes from NOAA’s CPC, available at: [https://www.cpc.ncep.noaa.gov/products/precip/CWlink/daily\\_ao\\_index/aao/aao.shtml#publication](https://www.cpc.ncep.noaa.gov/products/precip/CWlink/daily_ao_index/aao/aao.shtml#publication).

Before conducting comparisons, snow cover extent, precipitation, and streamflow were aggregated or averaged on either an annual or seasonal basis. Specific details are provided in the plot captions. We applied the Pearson Correlation Test to test whether two time series are linearly independent. A p-value, or probability value, of 0.05 or less suggests that the two time series are statistically significantly dependent. To test the significance of trends, we applied linear regression models and used a t-test to determine if the slope was significantly different from zero. A p-value of less than 0.05 indicated that the trend was statistically significant.

Streamflow data comes from Dirección General de Aguas (DGA), are available at <http://explorador.cr2.cl/>.

Datasets of precipitations come from the atmospheric reanalysis ERA5 produced by the European Centre for Medium-range Weather Forecasts (ECMWF), available at: <https://www.ecmwf.int/en/forecasts/datasets/reanalysis-datasets/era5>.

Weekly sea surface temperature (SST) anomalies in the Niño regions come from NOAA’s Climate Prediction Center (CPC), available at <https://www.cpc.ncep.noaa.gov/data/indices/wksst8110.for>.

Daily estimates of the SAM index are available at: [https://www.cpc.ncep.noaa.gov/products/precip/CWlink/daily\\_ao\\_index/ao/ao.shtml#publication](https://www.cpc.ncep.noaa.gov/products/precip/CWlink/daily_ao_index/ao/ao.shtml#publication).

## Data availability

Snow cover data are based on satellite-derived estimates from MODIS/Terra Snow Cover Daily L3 Global 500 m SIN Grid, version 6.1, available at <https://nsidc.org/data/mod10a1/versions/61Streamflow> data comes from Direccion General de Aguas (DGA), are available at <http://explorador.cr2.cl/Datasets> of precipitations come from the atmospheric reanalysis ERA5 produced by the European Centre for Medium-range Weather Forecasts (ECMWF), available at: <https://www.ecmwf.int/en/forecasts/datasets/reanalysis-datasets/era5> Weekly sea surface temperature (SST) anomalies in the Niño regions come from NOAA's Climate Prediction Center (CPC), available at <https://www.cpc.ncep.noaa.gov/data/indices/wksst8110>. Daily estimates of the SAM index are available at: [https://www.cpc.ncep.noaa.gov/products/precip/CWlink/daily\\_ao\\_index/ao/ao.shtml#publication](https://www.cpc.ncep.noaa.gov/products/precip/CWlink/daily_ao_index/ao/ao.shtml#publication).

Received: 27 March 2024; Accepted: 28 October 2024

Published online: 11 November 2024

## References

- Minora, U. et al. 2008–2011 snow covered area (SCA) variability over 18 watershed of the central Chile through MODIS data. *Geogr. Fis. Dinam. Quat.* **38**, 169–174 (2015).
- Masiokas, M. H. et al. Streamflow variations across the Andes (18–55 S) during the instrumental era. *Sci. Rep.* **9**(1), 17879 (2019).
- Garreaud, R. & Aceituno, P. Atmospheric circulation over South America: Mean features and variability. In *The Physical Geography of South America* (eds Veblen, T. et al.) (Oxford University Press, 2007).
- Viale, M., Valenzuela, R., Garreaud, R. D. & Ralph, F. M. Impacts of atmospheric rivers on precipitation in southern South America. *J. Hydrometeorol.* **19**(10), 1671–1687 (2018).
- Falvey, M. & Garreaud, R. Wintertime precipitation episodes in central Chile: Associated meteorological conditions and orographic influences. *J. Hydrometeorol.* **8**(2), 171–193 (2007).
- Garreaud, R. The Andes climate and weather. *Adv. Geosci.* **7**, 1–9 (2009).
- Masiokas, M. H. et al. A review of the current state and recent changes of the Andean cryosphere. *Front. Earth Sci.* **8**, 99 (2020).
- Cortés, G. & Margulis, S. A. Impacts of El Niño and La Niña on interannual snow accumulation in the Andes: Results from a high-resolution 31 year reanalysis. *Geophys. Res. Lett.* **44**, 6859–6867 (2017).
- Cortés, G., Giroto, M. & Margulis, S. A. Analysis of sub-pixel snow and ice extent over the extratropical Andes using spectral unmixing of historical landsat imagery. *Remote Sens. Environ.* **141**, 64–78 (2014).
- Cordero, R. R. et al. Dry-season snow cover losses in the Andes (18–40 S) driven by changes in large-scale climate modes. *Sci. Rep.* **9**(1), 16945 (2019).
- Malmros, J. K., Mernild, S. H., Wilson, R., Tagesson, T. & Fensholt, R. Snow cover and snow albedo changes in the central Andes of Chile and Argentina from daily MODIS observations (2000–2016). *Remote Sens. Environ.* **209**, 240–252 (2018).
- Saavedra, F. A., Kampf, S. K., Fassnacht, S. R. & Sibold, J. S. Changes in Andes snow cover from MODIS data, 2000–2016. *Cryosphere*. **12**, 1027–1046 (2018).
- Barria, I., Carrasco, J., Casassa, G. & Barria, P. Simulation of long-term changes of the equilibrium line altitude in the central Chilean Andes Mountains derived from atmospheric variables during the 1958–2018 period. *Front. Environ. Sci.* **7**, 161 (2019).
- Hammond, J. C., Saavedra, F. A. & Kampf, S. K. Global snow zone maps and trends in snow persistence 2001–2016. *Int. J. Climatol.* **38**(12), 4369–4383 (2018).
- NOAA. National Centers for Environmental Information. Climate Prediction Center (CPC), Equatorial Pacific Sea Surface Temperatures. Available at, (2023)., October 12 <https://www.ncdc.noaa.gov/teleconnections/ensio/indicators/sst/>. Accessed 21 Sept 2023.
- Montecinos, A. & Gomez, F. ENSO modulation of the upwelling season of southern-central Chile. *Geophys. Res. Lett.* **37**(2), (2009).
- Valdés-Pineda, R., Valdes, J. B., Diaz, H. F. & Pizarro-Tapia, R. Analysis of spatio-temporal changes in annual and seasonal precipitation variability in South America-Chile and related ocean–atmosphere circulation patterns. *Int. J. Climatol.* **36**(8), 2979–3001 (2016).
- Mo, K. C. Relationships between low-frequency variability in the Southern Hemisphere and Sea Surface temperature anomalies. *J. Clim.* **13**, 3599–3610 (2000).
- Jones, J. M. et al. Assessing recent trends in high-latitude Southern Hemisphere surface climate. *Nat. Clim. Chang.* **6**, 917–926 (2016).
- Marshall, G. J. Trends in the Southern Annular Mode from observations and reanalyses. *J. Clim.* **16**, 4134–4143 (2003).
- Boisier, J. P. et al. Anthropogenic drying in central-southern Chile evidenced by long-term observations and climate model simulations. *Elem. Sci. Anth* **6**, (2018).
- Damiani, A. et al. Connection between Antarctic ozone and climate: Interannual precipitation changes in the Southern Hemisphere. *Atmosphere* **11**, 579 (2020).
- Garreaud, R. D. et al. The central Chile mega drought (2010–2018): A climate dynamics perspective. *Int. J. Climatol.* **40**(1), 421–439 (2020).
- Hall, D. K. & Riggs, G. A. Accuracy assessment of the MODIS snow products. *Hydrol. Process.* **21**(12), 1534–1547 (2007).
- Muñoz, A. A. et al. Water crisis in Petorca Basin, Chile: The combined effects of a mega-drought and water management. *Water* **12**(3), 648 (2020).
- Thompson, D. W. & Solomon, S. Interpretation of recent Southern Hemisphere Climate change. *Science* **296**, 895–899 (2002).
- Banerjee, A., Fyfe, J. C. & Polvani, L. M. A pause in Southern Hemisphere circulation trends due to the Montreal Protocol. *Nature* **579**, 544–548 (2020).
- Fogt, R. L., Bromwich, D. H. & Hines, K. M. Understanding the SAM influence on the South Pacific ENSO teleconnection. *Clim. Dyn.* **36**, 1555–1576 (2011).
- Wiegel, H. Complicating the tale of ‘first climate migrants’: Resource-dependent livelihoods, drought and labour mobilities in semi-arid Chile. *Geoforum*. **138**, 103663 (2023).
- Cordero, R. R. et al. UV Irradiance and Albedo at Union Glacier Camp (Antarctica): A case study. *PLoS ONE* **9**(3), (2014).
- Alfonso, J. A. et al. Elemental and mineralogical composition of the western Andean snow (18° S–41° S). *Sci. Rep.* **9**, 1–13 (2019).
- Rowe, P. M. et al. Black carbon and other light-absorbing impurities in snow in the Chilean Andes. *Sci. Rep.* **9**, 1–16 (2019).
- Cordero, R. R. et al. Black carbon in the Southern Andean snowpack. *Environ. Res. Lett.* **17**(4), 044042 (2022).
- Garreaud, R. D., Clem, K. & Veloso, J. V. The South Pacific pressure trend dipole and the southern blob. *J. Clim.* **34**(18), 7661–7676 (2021).

35. Kwon, H. et al. Recent weakening of the southern stratospheric polar vortex and its impact on the surface climate over Antarctica. *Environ. Res. Lett.* **15**(9), 094072 (2020).
36. Cordero, R. R. et al. Signature of the stratosphere-Troposphere coupling on recent record-breaking Antarctic Sea ice anomalies. *Cryosphere* **17**, 4995–5006 (2023).
37. Byrne, N. J. & Shepherd, T. G. Seasonal persistence of circulation anomalies in the Southern Hemisphere stratosphere and its implications for the Troposphere. *J. Clim.* **31**(9), 3467–3483 (2018).
38. Cai, W. et al. Increased variability of eastern Pacific El Niño under greenhouse warming. *Nature* **564**, 201–206 (2018).
39. Wang, G. et al. Continued increase of extreme El Niño frequency long after 1.5 C warming stabilization. *Nat. Clim. Chang.* **7**, 568–572 (2017).
40. Lim, E. P. et al. The impact of the Southern Annular Mode on future changes in Southern Hemisphere rainfall. *Geophys. Res. Lett.* **43**, 7160–7167 (2016).
41. Deng, K. et al. Changes of Southern Hemisphere westerlies in the future warming climate. *Atmos. Res.* **270**, 106040 (2022).
42. Hall, D. K. & Riggs, G. A. MODIS/Terra Snow Cover Daily L3 Global 500m SIN Grid, Version 61. [Indicate subset used]. Boulder, Colorado USA. NASA National Snow and Ice Data Center Distributed Active Archive Center. (2021). <https://doi.org/10.5067/MODIS/MOD10A1.061>. Accessed: 13 Nov 2023.
43. Hall, D. K., Riggs, G. A., DiGirolamo, N. E. & Román, M. O. Evaluation of MODIS and VIIRS Cloud-gap-filled snow-cover products for production of an Earth science data record. *Hydrol. Earth Syst. Sci.* **23**(12), 5227–5241 (2019).
44. Härer, S., Bernhardt, M., Siebers, M. & Schulz, K. On the need for a time- and location-dependent estimation of the NDSI threshold value for reducing existing uncertainties in snow cover maps at different scales. *Cryosphere* **12**(5), 1629–1642 (2018).
45. Salomonson, V. V. & Appel, I. Estimating fractional snow cover from MODIS using the normalized difference snow index. *Remote Sens. Environ.* **89**(3), 351–360 (2004).
46. Crespo, S. A. et al. Where does the Chilean Aconcagua river come from? Use of natural tracers for water genesis characterization in glacial and periglacial environments. *Water* **12**(9), 2630 (2020).
47. Rodriguez, E. et al. An assessment of the SRTM topographic products, Technical Report JPL D-31639 143 (Jet Propulsion Laboratory, 2005).
48. Hersbach, H. The ERA5 atmospheric reanalysis AGUFGM, NG33D-01 (2016).
49. Hunter, J. D. & Matplotlib A 2D graphics environment. *Comput. Sci. Eng.* **9**, 90–95 (2007).

## Acknowledgements

We thank the Direccion General de Aguas (DGA), the European Centre for Medium-Range Weather Forecasts (ECMWF), NOAA's Climate Prediction Center (CPC), and the MODIS team for the data access as well as all their hard work in producing the datasets. The support of ANID (ANILLO ACT210046) and VRIIC-DICYT (092431CC\_Ayudante) is gratefully acknowledged.

## Author contributions

Conceived and designed the experiments: R.R.C., S.F., G.C.; Performed the experiments: R.R.C., S.F., J.J., E.S.; Analyzed the data: R.R.C., S.F., S.M., F.C., J.C.; Contributed materials/analysis tools: R.R.C., S.F., A.D., J.P., F.F., C.W., A.K.; Wrote the paper: R.R.C., S.F., A.D., J.C., C.K., E.S., C.W.

## Declarations

## Competing interests

The authors declare no competing interests.

## Additional information

**Supplementary Information** The online version contains supplementary material available at <https://doi.org/10.1038/s41598-024-78014-0>.

**Correspondence** and requests for materials should be addressed to S.F.

**Reprints and permissions information** is available at [www.nature.com/reprints](http://www.nature.com/reprints).

**Publisher's note** Springer Nature remains neutral with regard to jurisdictional claims in published maps and institutional affiliations.

**Open Access** This article is licensed under a Creative Commons Attribution-NonCommercial-NoDerivatives 4.0 International License, which permits any non-commercial use, sharing, distribution and reproduction in any medium or format, as long as you give appropriate credit to the original author(s) and the source, provide a link to the Creative Commons licence, and indicate if you modified the licensed material. You do not have permission under this licence to share adapted material derived from this article or parts of it. The images or other third party material in this article are included in the article's Creative Commons licence, unless indicated otherwise in a credit line to the material. If material is not included in the article's Creative Commons licence and your intended use is not permitted by statutory regulation or exceeds the permitted use, you will need to obtain permission directly from the copyright holder. To view a copy of this licence, visit <http://creativecommons.org/licenses/by-nc-nd/4.0/>.

© The Author(s) 2024